Mon. Not. R. Astron. Soc. **000**, 1–**??** (2002) Printed 2 February 2008 (MN LaTeX style file v2.2)

arXiv:astro-ph/0302416v1 20 Feb 2003

Continuum and spectral line observations of the OH Megamaser galaxy Arp 220

E. Rovilos[1]⋆, P. J. Diamond[1], C. J. Lonsdale[2], C. J. Lonsdale[3] and H. E. Smith[4]
[1] *Jodrell Bank Observatory, University of Manchester, Macclesfield, Cheshire, SK11 9DL, U.K.*
[2] *MIT Haystack Observatory, Off Route 40, Westford, MA 01886, U.S.A.*
[3] *Infrared Processing and Analysis Center, California Institute of Technology, 100 22, Pasadena, CA 91125, U.S.A.*
[4] *Center for Astrophysics and Space Sciences, University of California, San Diego, La Jolla, CA 92093-0424, U.S.A.*

2 February 2008

ABSTRACT
We present MERLIN observations of the continuum (both 1.6 and 5 GHz) and OH maser emission towards Arp 220. The correct spatial configuration of the various components of the galaxy is revealed. In the eastern component the masers are shown to be generally coincident with the larger-scale continuum emission; in the west, the masers and continuum do not generally arise from the same location. A velocity gradient ($(0.32\pm0.03)\,\mathrm{km\,s^{-1}pc^{-1}}$) is found in the eastern nuclear region on MERLIN scales; this gradient is three times smaller than that seen in HI and implies that the OH gas lies inside the HI. A re-analysis of previously presented global VLBI data (Lonsdale et al. 1998) reveals a very high velocity gradient ($(18.67\pm0.12)\,\mathrm{km\,s^{-1}pc^{-1}}$) in one component, possibly the site of a heavily obscured AGN.

Key words: masers – galaxies:individual:Arp220 – galaxies:active – radio continuum:galaxies – radio lines:galaxies.

1 INTRODUCTION

Ultra-luminous infrared galaxies (ULIRGs) are so named because their infrared luminosity is greater than the luminosity in all the other wavelengths combined ($L_{IR} > 10^{12} L_{\odot}$). The source of such copious emission is thought to be the enormous amount of molecular dust in their central regions, which obscures visible and other wavelengths and produces infrared light through heating. The dust grains are excellent absorbers of short wavelength radiation emitted from newly formed OB stars, so a high infrared luminosity is a tracer of star formation. In many cases however active galactic nuclei and Seyfert-like nuclei can play an important role. A review of the properties of this kind of galaxy can be found in Sanders & Mirabel (1996).

One of the most interesting properties of ULIRGs is that they tend to be merging systems, as it takes a strong merger of dust rich galaxies to generate the observed high density star formation. The proportion of the mergers among ULIRGs gets larger when the infrared luminosity gets higher, and is 100% in luminosities above $10^{12} L_{\odot}$. (See Sanders & Mirabel (1996) and references therein). Many of them also have very powerful OH maser emission (e.g. Darling & Giovanelli (2002)) in which the luminosity exceeds that of known galactic masers by a factor of at least 10^6, hence the term "megamaser".

Arp 220 is one of the most luminous infrared galaxies with $L_{IR} = 1.4 \times 10^{12} L_{\odot}$ (Soifer et al. 1987) and provides a superb example of the starburst phenomenon, demonstrated graphically by the discovery of several radio supernovae (Smith et al. 1998). Starburst phenomena are used by Shioya, Trentham & Tanigushi (2001) and Iwasawa et al. (2001) to explain the X-ray properties of Arp 220, although the existence of a heavily obscured AGN is not ruled out. Recent CHANDRA results (Clements et al. 2002) show that the hard X-Ray emission in Arp 220 is confined in a sub-kiloparsec scale region, in contrast to other starburst galaxies and its spectrum shows that the hard X-rays are more likely to be produced by one or more low luminosity, heavily obscured AGN, X-Ray binaries or Ultra Luminous X-Ray sources rather than the supernovae. Therefore the co-existence of such structures is still plausible.

The morphology of Arp 220 is also an open issue. At optical (Scoville et al. 1998) as well as at radio wavelengths (eg. Norris 1988) it exhibits a double structure with tidal tails and dust lanes which leads to the assumption that it is the result of a recent merging phenomenon. Studies of CO, HI and the OH maser emission enable the determination of its velocity structures. On balance, the current data appear to favor a model of two counterrotating disks as parts of a larger scale disk (Sakamoto et al. 1999; Mundell, Ferruit & Pedlar 2001), but a single warped circumnuclear disk model can also be fit to the data (Eckart & Downes 2001). In the case of the related galaxy IIIZw35 the existence of evidence for such a disk, where the OH maser is located, was recently revealed (Philström et al. 2001) so a search for a similar structure in Arp 220 would be useful.

The very powerful maser emission is perhaps the most

⋆ E-mail: erovilos@jb.man.ac.uk

striking property of Arp 220. It was first discovered by Baan, Wood & Haschick (1982) while searching for OH absorption in galaxies with known HI absorption. The masers were thought to arise in regions extending to several hundreds of parsecs (Baan 1985). However, higher resolution studies (Diamond et al. 1989; Lonsdale et al. 1998) revealed a dual component structure: there is a diffuse component which consists of approximately one third of the 1667 MHz OH emission plus almost all of the 1665 MHz OH emission with a physical extent of some hundred parsecs as suggested by the Baan model; but there is also a compact component consisting only of the 1667 MHz line with a physical extent of just a few parsecs. These compact masers show high velocity widths, even in this very small physical extent (Lonsdale et al. 1998). This means that either they come from a region with a volume of a few pc^3 or they represent long, thin filaments with their orientation along the line of sight. In the first case there has to be a hidden infrared source in that region to provide the essential pumping photons, or the optical depth of this region has to be large enough to trap the infrared photons, if the pumping is indeed radiative and not collisional due to shock fronts from the nearby supernovae. If filamental structure was present to any great extent we would have to explain why the filaments' orientation is only along the line of sight, so that we cannot see elongated structures (Lonsdale et al 2001). Probably we are only seing filaments which lie on the line of sight due to the gain path needed for a maser to be detected.

In this paper we present new MERLIN OH spectral line and continuum data, and compare it with previously presented global VLBI data (Smith et al. 1998; Lonsdale et al. 1998).

2 OBSERVATIONS AND DATA REDUCTION

In this section we describe the MERLIN and global VLBI observations of both line and continuum emission

2.1 MERLIN Observations

2.1.1 1.6 GHz Spectral Line Data

Data were taken on 23 April 1998 with seven MERLIN antennas including the 76 m Lovell telescope observing with left-hand circular polarization only. The dataset included observations of the target source Arp 220 (spending 9 hours and 20 minutes on source) and the phase reference 1511+238, as well as two scans on the point source calibrator 2134+004 and one scan on the flux calibrator 3C286. The observations covered a bandwidth of 4 MHz and were correlated to produce 256 channels, each with a bandwidth of 15.625 KHz.

The initial editing and gain elevation corrections, as well as preliminary amplitude calibration were made using MERLIN specific software. Then, the data were transferred into NRAO's Astronomical Image Processing System (AIPS) for bandpass calibration and phase corrections. Phase referencing was performed using the data on 1511+238. The data were then self-calibrated starting from a point source model and the solutions were applied to the Arp 220 data. After that line free channels were averaged and an image of this continuum was produced in 'difmap'. There may be modest contamination of the continuum image by weak 1665 MHz OH emission but tests have shown this to be minimal. We attempted to image the 1665 MHz emission but it was too diffuse even on MERLIN scales; it was detected only on short baselines, shorter than $0.35\,M\lambda$. Several iterations of self-calibration were performed on the continuum data and the solutions obtained were then applied to the multi-frequency dataset and the data averaged for 60 seconds. The final spectral line dataset was generated by subtracting the continuum emission using UVLIN and then averaging every two channels together, resulting in a velocity resolution of $5.6\,\mathrm{km\,s^{-1}}$.

2.1.2 1.6 GHz Continuum Data

Continuum data were taken on 23 June 1998 with six MERLIN antennas using right hand circular polarization. The dataset includes observations of the target source Arp 220 (spending 4 hours on source) and the phase reference 1511+238, as well as two scans on the point source calibrator 2134+004 and two scans on the flux calibrator 3C286. 16 channels were generated by the correlator, each with a bandwidth of 1 MHz, the central channel (8) being set at a frequency of 1666.00 MHz.

Local MERLIN software was used to perform the gain elevation corrections and preliminary amplitude calibration and editing. Bandpass calibration was performed and AIPS was used for further calibration. After flux calibration, the phase reference source was used for phase calibration, and three rounds of self-calibration were performed on 1511+238 starting from a point-source model. The solutions were copied and applied to all the data, channels 2 to 15 were averaged and a first image of Arp 220 was produced. Starting from this image, we performed four iterations of self calibration on the Arp 220 data before creating the final image.

2.1.3 5 GHz Continuum Data

5 GHz data were taken using 6 MERLIN antennas in full polarization on 29 May 2000. The dataset consisted of observations of Arp 220 (spending 7 hours on source) and the phase reference 1551+239 as well as five scans on the point source 2134+004 and two scans on the flux calibrator 3C286. Again, 16 channels were produced by the correlator each with a bandwidth of 1 MHz, the central channel being set at a frequency of 4.995 GHz.

Standard procedures were followed for the data reduction, the phase corrections from the phase reference source were applied to the Arp 220 data and after self-calibration the final image was produced using Stokes I.

2.2 VLBI Observations

The VLBI data used for comparison are those discussed in our previous papers, Smith et al. (1998) and Lonsdale et al. (1998). The data were taken in November 1994 and discussion of the calibration is contained with the papers.

3 RESULTS

3.1 Continuum

3.1.1 MERLIN

The 1.6 GHz (June 1998) MERLIN continuum image of Arp 220 is shown in Figure 1: A double component structure is present, with the western and the eastern components separated by $\sim$1 arcsec ($\sim$370 pc if we assume a distance of 76 Mpc; $\mathrm{H_0}$=75 $\mathrm{km\,s^{-1}\,Mpc^{-1}}$) and at the same positions as the 1.3 mm (Sakamoto et al. 1999) and the 4.83 GHz (Baan & Haschick 1995; this paper) continuum peaks. The integrated flux densities are

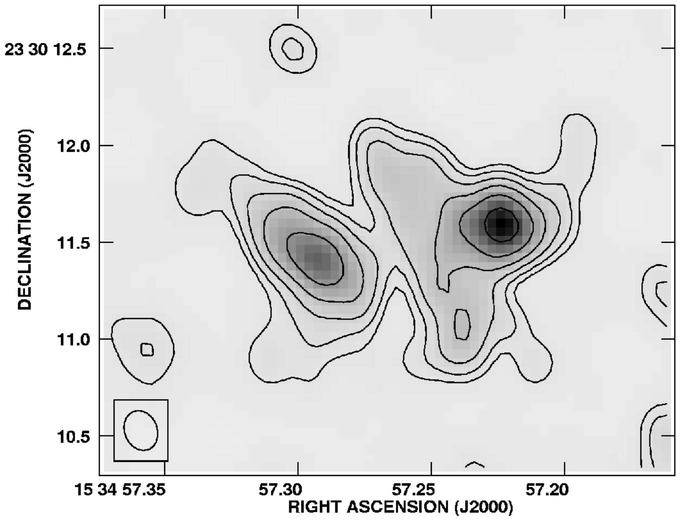

Figure 1. The 1.6 GHz image of Arp 220 from the MERLIN continuum data. The peak flux is 44.604 mJy beam^{-1} and the contour levels are at 1, 2, 4, 8, 16 and 32 mJy. The beam size is shown at the bottom left corner of the image and is 209.97×167.48 mas (77.4×61.7 pc) and the off source noise level is 055 mJy beam^{-1}.

(91.9±0.9) mJy and (111.2±0.8) mJy for the eastern and the western components respectively. We should note here that the component boundaries are somewhat arbitrary, so the overall diffuse emission plays a role in deriving these numbers: the values given are lower limits. The total integrated flux density of the galaxy at 1.6 GHz is (280±40) mJy, consistent with that derived at 1.4 GHz by Mundell et al. (2001) (285.4±14.3 mJy).

In Figure 1 we can see that the eastern component is elongated in a northeast - southwest direction and a ‘spur’ of emission is visible on the northwest of the western component. This is also detected by Mundell et al. (2001) at 1.4 GHz and by Baan & Haschick (1995) in the 4.8 GHz continuum. A component southeast of the western component is also detected as part of a more extended emission pattern, possibly part of the extended emission detected by the VLA (Baan & Haschick 1984). The peak flux of this region is 8.72 mJy beam^{-1}, whereas the off-source noise level is 0.55 mJy beam^{-1}.

In Figure 2 we can see the 5 GHz image of Arp 220 where again the double component structure is present, although more extended structure is not detected. The peaks of the two components are separated by (1.066±0.004) arcsec and their integrated fluxes are (33.6±1.0) mJy and (60.7±0.8) mJy for the east and west respectively, while the off-source noise level is 0.4 mJy beam^{-1}. If we compare these fluxes with these of the 1.6 GHz data we can derive the spectral indices of these two continuum components to be:

$\alpha_e = -0.90 \pm 0.03$

$\alpha_w = -0.542 \pm 0.013$

The errors shown here are statistical. There might be systematic effects that cause larger errors. The spectral indices derived here are similar to the spectral index (for the whole nucleus) assumed by Norris (1988) (-0.6 to -0.9). This is a characteristic of synchrotron radiation (see next paragraph) though it cannot give us a safe indication of the exact origin of the emission or its power source.

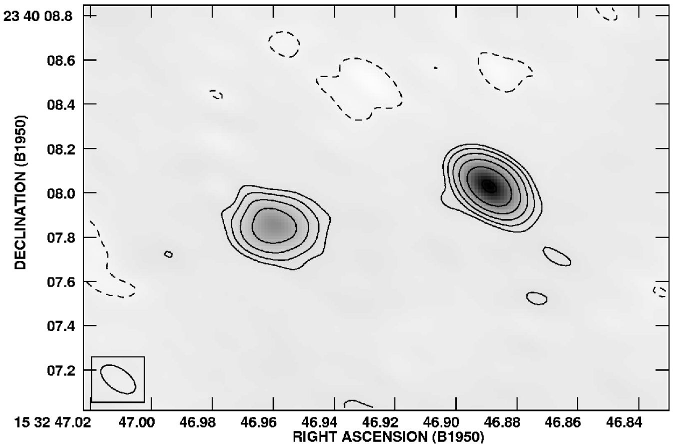

Figure 2. The 5 GHz image of Arp 220 from the MERLIN continuum data. The peak flux is 34.6 mJy beam^{-1} and the contour levels are at 1, 2, 4, 8, 16, and 32 mJy, as in Figure 1. The beam size is shown at the bottom left corner of the image and is 178.42×95.16 mas (65.7×35.1 pc). The off-source noise level is 0.4 mJy beam^{-1}.

3.1.2 Global VLBI

The results from the continuum VLBI dataset have been previously presented by Smith et al. (1998), where the discovery of probable radio supernovae (RSNe) is reported. There are about a dozen RSNe (November 1994) in the western nuclear region and possibly one or two in the eastern, without any other obvious compact continuum component. (Figures 1a and 1b respectively in Smith et al. (1998)) The sum of the flux densities of the observed supernovae in the western region is 7.87 mJy and in the eastern is 0.78 mJy including the marginally detected ones. If we compare these with the flux densities observed with MERLIN it is safe to assume that the MERLIN and VLBI continuum detections are the results of different processes; the large-scale MERLIN continuum emission probably comes from synchrotron acceleration of free electrons (possibly generated in the supernova explosions), while the VLBI emission probably arises from the interaction between the explosion material and the stellar wind generated before the star exploded.

3.2 Spectral Line

3.2.1 MERLIN

The naturally weighted velocity maps of Arp 220 (after continuum subtraction) can be seen in Figure 3. There are three components present, one in the east and two in the west (northwest and southwest). The eastern component is more redshifted than those in the west, suggesting an overall velocity gradient along the east-west axis. This is in agreement with the suggested presence of an overall rotating disk (Scoville, Yun & Bryant 1997; Sakamoto et al. 1999; Mundell et al. 2001). The off-source noise level is 3.2 mJy beam^{-1}.

In Figure 4 we can see the spectral line emission (naturally weighted and averaged over the velocity range of the OH emission) superimposed on the continuum emission. This continuum image (in greyscale) is not the same as that in Figure 1, but was generated from the continuum portion of the spectral line dataset. The error in relative position between the continuum and the spectral line image is less than a milliarcsecond but the noise in this continuum image is significantly greater than that obtained from the wideband continuum data (0.83 mJy beam^{-1}). The eastern portion of the spectral

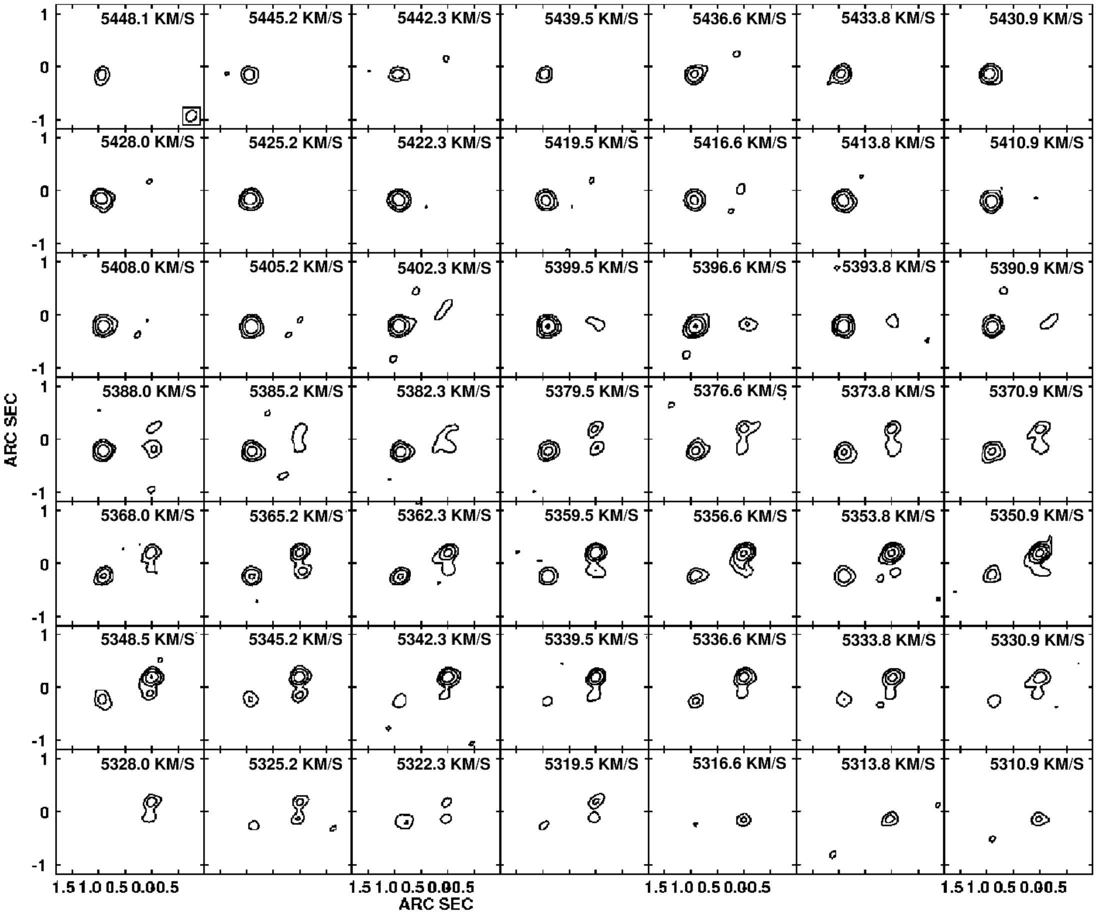

Figure 3. The natural weighted images of Arp 220 from the MERLIN spectral line data. The peak integrated flux is 166.73 mJy beam^{-1}. The beam size is shown at the bottom right corner of the first image and is 229.96×182.75 mas (84.7×67.3 pc). The noise level of each image is 3.2 mJy beam^{-1}.

line emission is seen to be at the same position as the continuum, but the peak of the western component of the continuum emission lies between the two regions of spectral line emission. The northwestern line component is at the same position as the compact VLBI component and the southwestern emission corresponds to the previously observed diffuse component (Lonsdale et al. 1998). The eastern component spectrum is broad and has a double peak, which implies that regions with different velocities are superimposed (visible with the VLBI) to produce the component detected with MERLIN; their spectra are blended together.

3.2.2 Global VLBI

Lonsdale et al. (1998) presented the results of the VLBI spectral line dataset, where they find both a diffuse and a compact component in each of the eastern and the western regions. In Figure 5 we can see the spectral line VLBI image of Arp 220 (in contours) with respect to the continuum emission (in greyscale). Both images are convolved with a taper of 10 Mλ to include both regions in one map, so they are of degraded spatial resolution. In the western region we can detect the maser in regions where we have continuum emission due to the supernovae, but the majority of the compact maser emission is detected in regions north and south of the supernovae, where no compact continuum is detected. In the case of the eastern region there is no clear compact continuum emission, only hints of possible radio supernovae; the maser does not follow the pattern seen in the west. Close-ups of the two nuclear regions are shown in contours (the same as in figures 1 and 2 of Lonsdale et al. (1998)) with full resolution. (Beam size 9.8×2.5 mas). Spectra of different regions are also shown. One interesting point to note is the fourth spectrum (lower left in Figure 5), which shows absorption. We should note that there are problems with imaging diffuse emission with the global VLBI due to the lack of short uv spacings, we are however confident of some absorption being present. This suggests that the OH radical is present even in regions with no maser emission. We also detect part of the 1665 MHz emission, clearly seen in the two diffuse regions (spectra 5 and 8) and in the eastern compact region (spectra 1 and 2). To determine the origin of this emission we used tighter boxes to determine the spectra; the 1665 MHz emission then fades dramatically with respect to the 1667 MHz emission. This suggests that it is diffuse and comes from the overall area, a result first reported in Lonsdale et al. (1998).

4 DISCUSSION

4.1 Positions of the Masers

Any discussion of positions must be prefaced by the comment that since we performed self calibration, information about the absolute positions of the components is lost. The conclusions we make below are based on the relative positions of the components. We have extremely accurate relative positions (sub-mas) since we are able

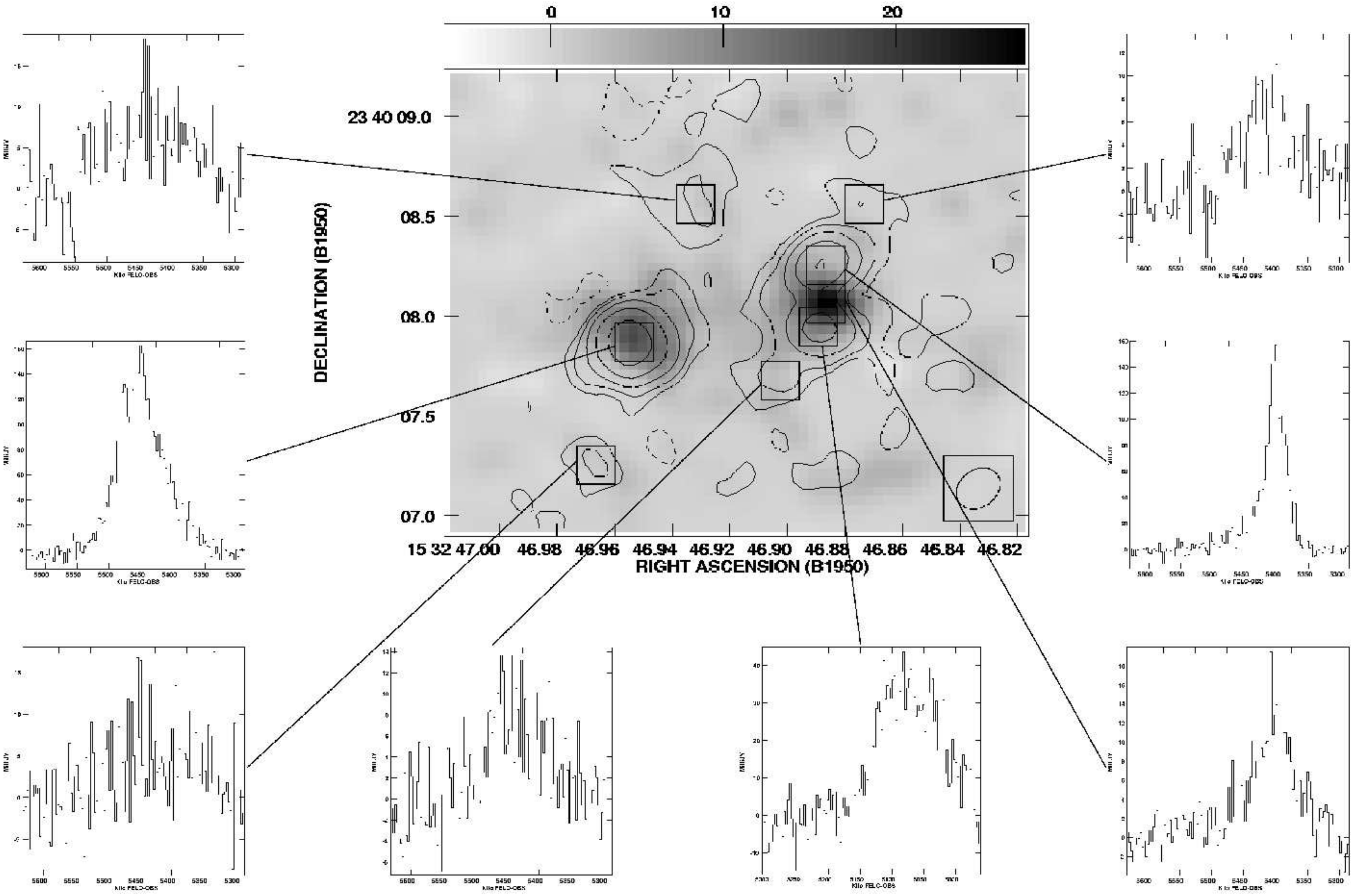

Figure 4. The continuum and spectral line images from the MERLIN spectral line dataset. The greyscale image is the continuum image found from line-free channels and the contours represent the maser emission. To make this image we averaged all the velocities (5326.7 – 5579.6 km s^{-1}) of the naturally weighted images. The boxes indicate the location of each spectrum.

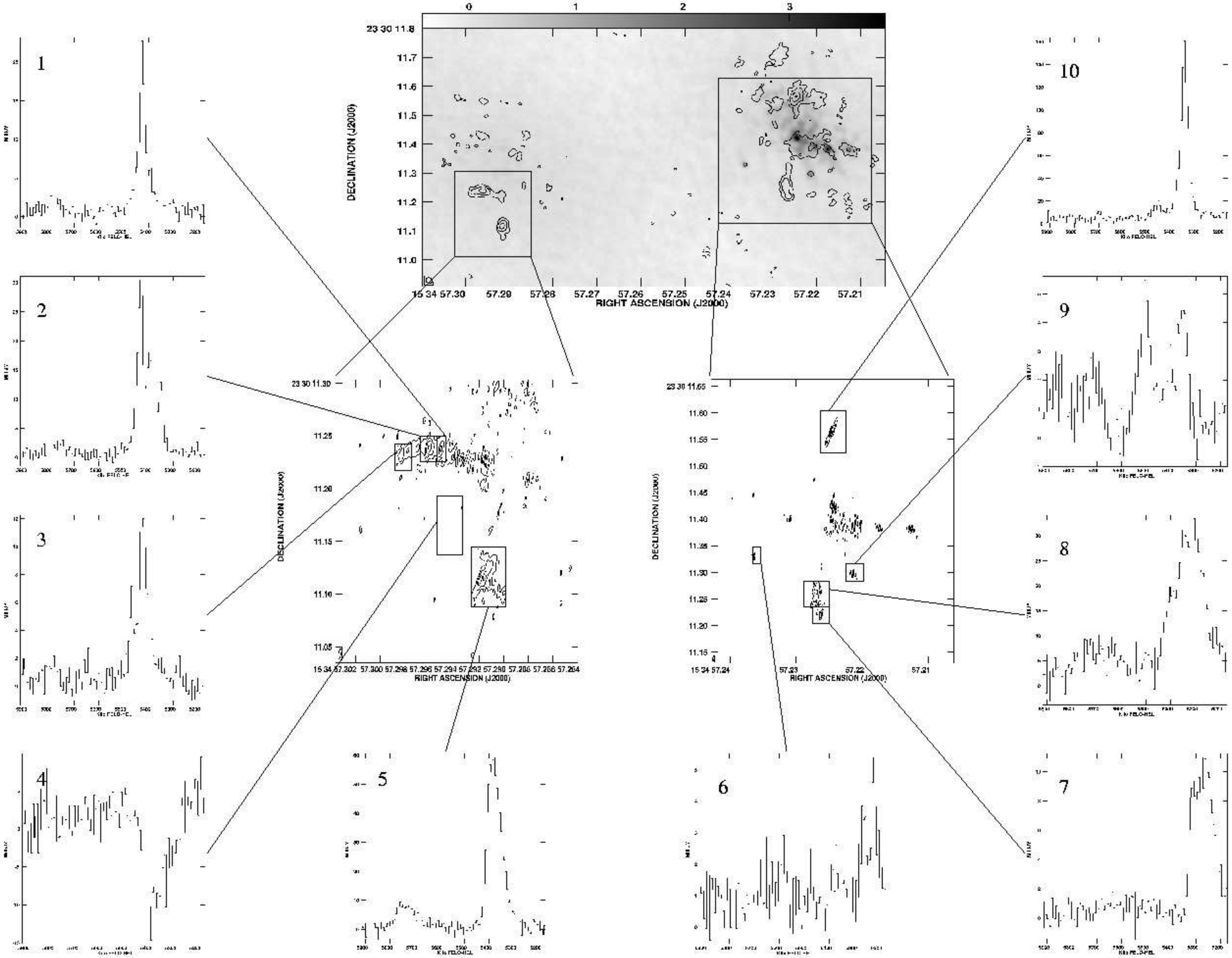

Figure 5. The continuum and spectral line images of Arp 220 from the global VLBI dataset. The greyscale map is the continuum with a convolved beam size of 19.7×17.3 mas and the contours show the maser emission with the same beam size. The beam is shown on the bottom left of the image. Close-ups are shown of the maser emission only with contours, representing 12, 24, 48 and 96% of the peak integrated flux, which is 1.24 mJy beam^{-1} for the left picture and 10, 20, 40 and 80% of the peak integrated flux, which is 2.59 mJy beam^{-1} for the right picture. The beam size is shown at the bottom left corner of each picture and is 9.8×2.5 mas (3.61×0.92 pc) for both pictures. The boxes in each picture indicate the region from which the spectrum was taken.

		δRA (arcsec)	δDEC (arcsec)
NW maser W cont	MERLIN	0.011±0.006	0.191±0.004
	VLBI	0.0024±0.0007	0.1394±0.0007
NW maser SW maser	MERLIN	-(0.012±0.011)	0.311±0.007
	VLBI	-(0.0335±0.0007)	0.3032±0.0016
W cont SW maser	MERLIN	-(0.022±0.008)	0.12±0.02
	VLBI	-(0.0359±0.0012)	0.1638±0.0017
NW maser E maser	MERLIN	-(0.993±0.006)	0.339±0.004
	VLBI	-(1.0710±0.0002)	0.3252±0.0006

Table 1. The positional differences between the individual components in both the MERLIN and VLBI spectral line and continuum emission.

to obtain low sensitivity images of the continuum emission from the spectral line datasets; these can be used to tie down the position of the high sensitivity continuum image with respect to the maser positions.

It is clear that in both MERLIN and VLBI maps the continuum emission does not coincide with the maser peaks. Table 1 lists the measured offsets between various maser and continuum components in the MERLIN and VLBI images. (We chose the brightest supernova as the location of the VLBI western continuum peak and the brightest maser component (area of spectrum 2) as the peak of the spectral line emission in the east).

From this table we can assume that the northwestern MERLIN component of the maser emission is at the same position as the compact northwestern VLBI maser component and the southwestern maser MERLIN component is at the same position as the diffuse southwestern VLBI maser component. In this case, the brightest radio supernova is on the northern part of the western MERLIN continuum emission, ∼0.05 arcsec offset from its center. In the eastern region, the VLBI maser emission is situated on the border of the MERLIN maser emission. Since the MERLIN maser and bulk of the continuum coincide within ∼0.07 arcsec, and the possible supernovae are situated in the area between the two VLBI maser components (Smith et al. 1998), they lie in the area of the MERLIN continuum emission.

Unfortunately, this registration of the different components in Arp 220 requires a revision of the alignment suggested by Mundell et al. (2001) (see their figure 8). We are confident that our alignment is correct, as we extracted both the continuum and line images of Figure 4 from the same dataset performing the same self calibration. This may, to some degree, affect their conclusions regarding the location of the supernovae within their tilted disc model.

4.1.1 Eastern Region

If we assume that the MERLIN 1.6 GHz continuum emission coincides with the 1.4 GHz continuum emission (Mundell et al. 2001), then all 1.6 GHz continuum, 1.4 GHz, 1.3 mm (Sakamoto et al. 1999) and 4.8 GHz (Baan & Haschick 1995) come from the same area, as does the HI absorption (Mundell et al. 2001) and CO emission (Sakamoto et al. 1999). Weak, tentatively detected supernovae are also situated there.

The MERLIN maser emission coincides with the continuum in the eastern component. The VLBI maser emission lies in regions with no obvious compact continuum background; it does not cover all the area covered by the MERLIN maser but is instead situated on the edge of this area having a face-on disk-like appearance. It is probably saturated; the lower limit of the amplification factor is 110 for the northern and 65 for the southern region (for the 1667 MHz line). However, the OH radical is present throughout the whole area, as exemplified by the detection of OH absorption.

4.1.2 Western Region

In the western region, the MERLIN 1.6 GHz, the 1.4 GHz, 4.8 GHz and 1.3 mm continuum emission come from the same area as the CO emission and HI absorption. The strong supernovae are situated there, close to the northern border, probably assisting the young OB stars in heating the dust grains. The position of the OH maser emission is however different. Both MERLIN and VLBI demonstrate that it arises from regions north and south of the continuum. The lower limit for the amplification factor (derived from the VLBI data) is 125 for the compact northern region, 45 for the southern diffuse region and 90 for the compact region on its southwest border, so that the two compact regions are very likely to be saturated. OH is present at some level throughout the western region; we can see some maser emission lying in front of two supernovae northeast and northwest from the diffuse maser region. However, the amplification factors at the line peaks in front of the supernovae are very small, 4.6±0.7 and 3.3±0.3 respectively. This means that they lie in the area of diffuse, low-amplifying OH gas, which we only can detect in those regions with significant continuum radiation. Observations with better sensitivity will be able to detect more sources of this kind and so study the properties of the diffuse OH in some detail.

4.2 Velocity Gradiens

Figure 6 shows the moment map taken from the MERLIN data. There is a clear velocity gradient of (0.32±0.03) km s^{-1}pc^{-1} in the eastern region, at a position angle of 35.5°. Mundell et al. (2001) find (1.01±0.02) km s^{-1}pc^{-1} for the HI at a PA of ∼55°. If we assume that the OH arises from a circular rotating disc, its radius is (79±5) pc and its dynamical mass is $(12\pm3)\times10^{6}$M$_\odot$. This is smaller by a factor of 90 than the mass of 1.1×10^{9}M$_\odot$ calculated from HI absorption. This large difference may be explained if the OH gas lies in the inner part of the disk and the HI and CO arise in the outer part. This disc may be warped, explaining the difference in position angle between the OH and HI gradients.

Mundell et al. (2001) and Sakamoto et al. (1999) find a clear velocity gradient in HI and CO in the western region of Arp 220, in a roughly horizontal direction. In the MERLIN image of the OH

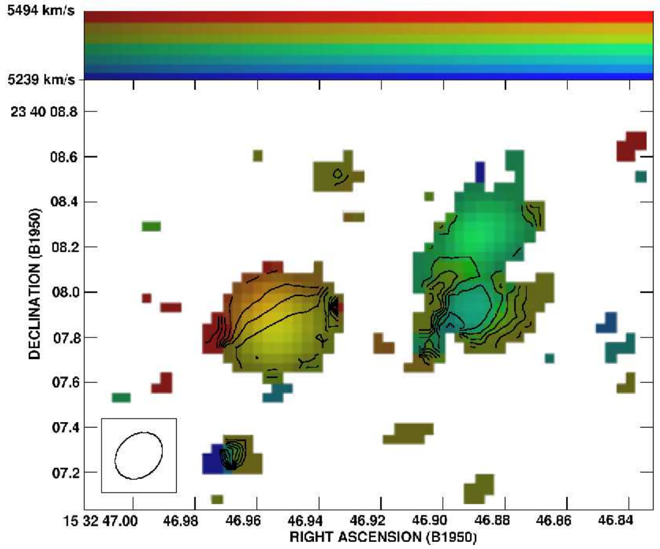

Figure 6. The moment map of Arp 220 from the MERLIN spectral line data. The intensity represents the flux density and the colors the velocity field, the reddest being the most redshifted. The contours represent the velocity field and they range from 5305 to 5475 $\mathrm{km\,s^{-1}}$ with spacings of 10 $\mathrm{km\,s^{-1}}$. The area selected to plot the velocity field is where the integrated flux is more than 15 $\mathrm{mJy\,beam^{-1}}$.

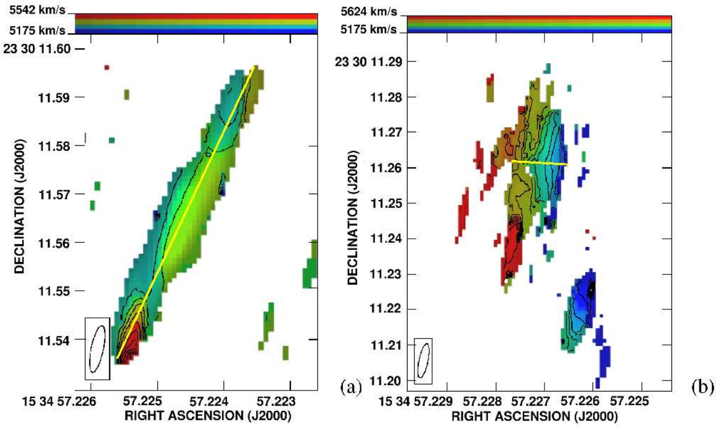

Figure 7. The moment maps of the western region of Arp 220 from the VLBI dataset. The left picture (a) represents the northern compact region and the right (b) the southern diffuse region. The contours for both pictures are 12.5 $\mathrm{km\,s^{-1}}$ apart, representing a velocity field from 5250 to 5612.5 $\mathrm{km\,s^{-1}}$. Only data whose integrated flux is greater than 1.5 $\mathrm{mJy\,beam^{-1}}$ are selected.

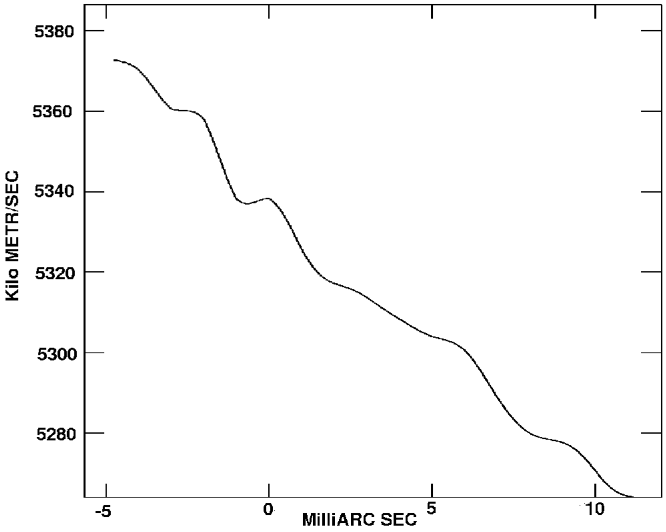

Figure 8. The velocity gradient of the southwestern region of Arp 220. The points from which the velocities were taken lie on the yellow line of Figure 7b with a position angle of 85.2°and no smoothing has been applied. The velocity gradient was derived using the least square method and is $(18.67\pm0.12)\,\mathrm{km\,s^{-1}pc^{-1}}$.

(Figure 6) we can see some velocity structure in the southwestern component, although a gradient is not clearly visible and in the northwestern component no gradient is detectable. However, the VLBI moment maps of Figures 7a and 7b (of the northern and southern region respectively) show that the southern component has a roughly E-W velocity gradient of $(18.67\pm0.12)\,\mathrm{km\,s^{-1}pc^{-1}}$ (Figure 8). The region from which this gradient arises is on the southern border of the region that contains the HI and CO gradient and its diameter is (5.9 ± 0.5) pc. If this gas was in rotation, the enclosed mass would be $(1.7\pm0.4)\times10^{7}\,\mathrm{M_{\odot}}$. The velocity gradient we measure is $\sim$20 times greater and the mass is $\sim$10 times smaller than that measured using HI absorption $(0.83\pm0.02)\,\mathrm{km\,s^{-1}pc^{-1}}$ and $1.7\times10^{8}\,\mathrm{M_{\odot}}$ respectively. A plausible explanation is that the OH is confined in a region of much smaller physical extent than the HI, in the center of the molecular disk. However, in comparison to the eastern region the mass is concentrated in the centre of the disk and that gives rise to the very high velocity gradient. Such a disk is however not well confined, so we cannot derive reliable results about the mass or determine how the density decreases with distance.

The northwestern component shows a very strange velocity structure. On the MERLIN scales no obvious structure is detected, whereas the VLBI structure can be seen in Figure 9. If we accept that the systemic velocity of this region is $\sim$5355 $\mathrm{km\,s^{-1}}$ (ie. the velocity of the central part of Figure 7a), then the region just outside and on both sides of the centre is blueshifted and it becomes redshifted as we go further out. Two possible explanations are proposed to explain this structure, the first being that the masing gas experiences spiral outflow within a cone, thus exhibiting an expanding helix structure (Figure 10). The problem with this configuration is that the velocity structure is symmetrical, so that one helix would be a mirror image of the other. Alternatively, there might be outgoing and ingoing spherical shock-waves producing the redshifted and blueshifted velocities (Figure 11). The observation of an elongated structure would be due to beaming effects.

To distinguish between these two proposed or other possible structures and investigate the nature of the central region higher spatial resolution observations have to be obtained, or a better signal-to-noise ratio has to be achieved. We will then be able to examine the velocity structure further away from the central point to see if it continues to be redshifted or instead becomes blueshifted again, something which would favor the outflow scenario.

4.3 Is There Still Room for an AGN?

When OH megamasers were first discovered, the question of whether a starburst or an AGN were providing the essential energy was raised. The discovery of RSNe in Arp 220 (Smith et al. 1998)

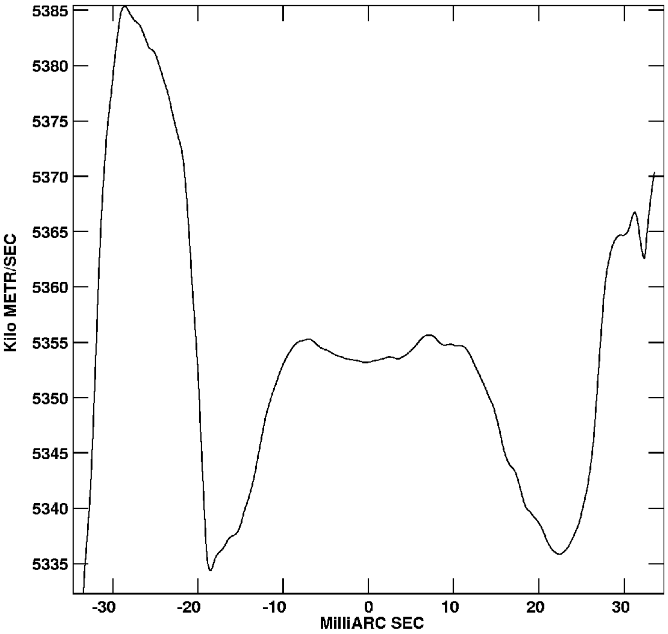

Figure 9. The velocity structure of the northwestern region of Arp 220. The different velocities are taken from points along the yellow line of Figure 7a which lies along the major axis of the emission. No smoothing has been applied.

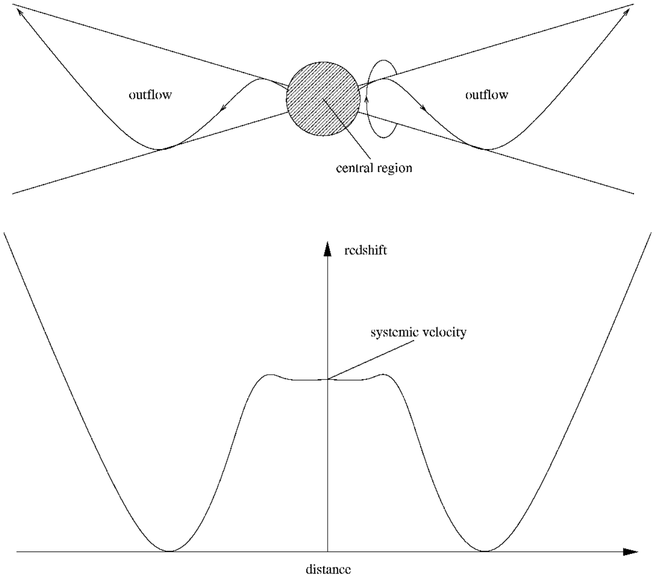

Figure 10. The expanding helix model as an explanation for the VLBI northwestern velocity structure. Note that the diagram and the sketch of the region are not in scale.

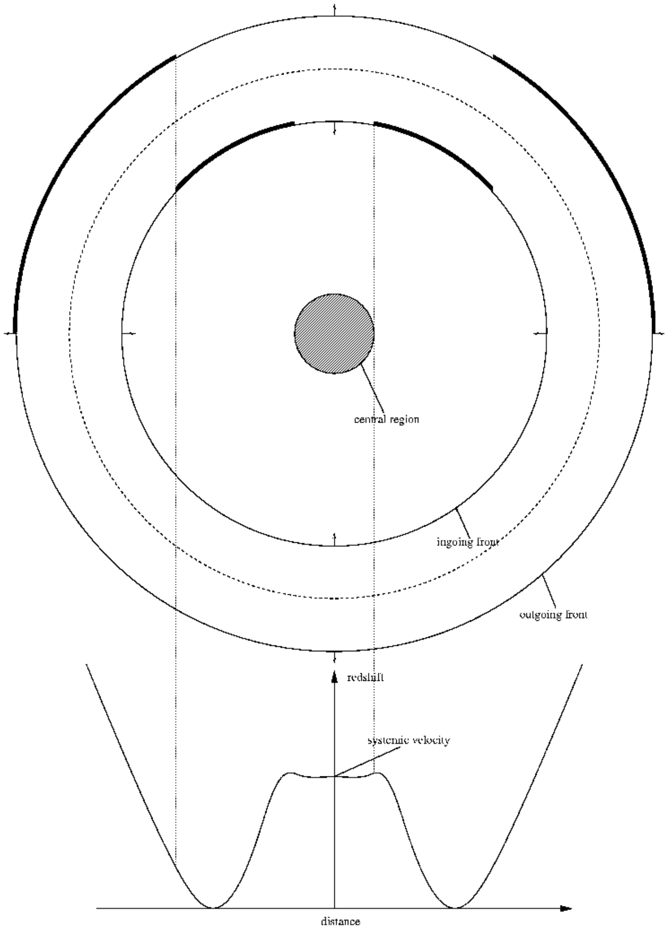

Figure 11. The double shock front scenario as an explanation of the northwestern area VLBI velocity structure. Bold lined indicate the regions which the masers we observe come from. The diagram and the sketch of the region are not in scale as in Figure 10.

answers this question in favour of the starburst. Luminous radio supernovae or nested supernovae remnants have since been tentatively detected in a number of OHMs (Mrk 273 (Carilli & Taylor 2000), IRAS 17028-0014 (Momjian et al. 2003 in preparation), Mrk 231 Taylor et al. (1999) and IIIZw35 (Philström et al. 2001)) linking the megamaser phenomenon with a nuclear starburst. The infrared luminosity is thought to arise from the vast amount of dust resulting from merging phenomena heated from young massive stars, whereas the radio continuum comes from relativistic electrons (partially generated from young stars and partially from supernova explosions) being accelerated by magnetic fields, so there is a correlation between the radio and the infrared fluxes (Bressan, Silva & Granato 2002).

An interesting common feature common of OH megamasers is that the emission comes from regions with clear velocity gradients, interpreted as molecular discs or torii. This is evident in Arp 220 (this paper), IIIZw35 (Philström et al. 2001), IRAS 17028-0014 (Momjian et al. 2003 in preparation), Mrk 273 (Yates et al. 2000) and Mrk 231 (Carilli, Wrobel & Ulvestad 1998). The formation of such a disc (or torus) is modeled by Barnes (2002) for merging gas-rich galaxies and a similar torus seems to be in agreement with high-resolution data of IIIZw35 (Philström et al. 2001). Given the high column densities of these regions ($8\times10^{19}\,T_s(K) < N_H < 2.4\times10^{20}\,T_s(K)\,cm^{-2}$ for Arp 220 HI (Mundell et al. 2001)) they can obscure low luminosity AGN. Indirect evidence in the form of a radio jet in Mrk 231 suggests that it hosts an AGN (Ulvestad et al. 1999). Compact hard X-ray sources in the nuclei of Arp 220 (Clements et al. 2002) and Mrk 273 (Xia et al. 2002) suggest that there is an active nucleus in those galaxies.

The existence of an AGN in OHM galaxies may well be a random phenomenon not associated with their masing properties, however statistical analysis of masing and non-masing LIRGs by Darling & Giovanelli (2002) reveals that LIRGs that host OH megamasers tend to be of infrared excess compared to those that don't. This means that there is another process taking place which contributes to the infrared flux and not the radio continuum. This can be a hidden AGN or a very recent starburst, which has not yet produced supernovae and relativistic electrons, OH megamasers can work as tracer for this kind of phenomena. To distinguish between the two possibilities one needs to model violent and sudden starbursts to check if the time scales until it starts contributing to the radio flux can explain the ratio of OHMs among LIRGs. Alternatively, a large number of OHMs and host galaxies should be observed with high sensitivity to determine if they host compact regions, candidates for hosting an AGN.

5 SUMMARY

Imaging of both the continuum and spectral line (OH) emission of Arp 220 using the same dataset has revealed the correct relative positions of its components. In the eastern radio nucleus the continuum and spectral emission coincide, whereas in the western the continuum is situated between the two spectral line emission peaks. On VLBI scales the continuum emission is in the form of several point sources, probably radio supernovae (Smith et al. 1998) in the same position as the MERLIN emission.

On large (MERLIN) scales the maser emission comes from three main regions, two western and one eastern. The eastern region has a very clear velocity gradient, showing rotation of the nuclear disc, if we follow the standard model (Sakamoto et al. 1999; Mundell et al. 2001). The velocity gradient we measure is significantly smaller than that found using HI absorption (Mundell et al. 2001). This may mean that the OH rotates inside the HI on large scales.

On smaller (VLBI) scales the OH maser emission has peculiar characteristics. In both nuclear regions the 1667 MHz line is emitted from regions of very small physical extent, whereas the 1665 MHz line seems to be of a more extended nature, coming from the overall region. Even on MERLIN scales (several hundred milliarcseconds) its location and structure could not be reliably determined. The most luminous maser is situated in the northwestern region and its velocity structure (Figure 9) implies that it either has a cone-like structure, which could be the result of molecular outflow from the central region or that it is produced by a pair of ingoing and outgoing shock fronts.

The issue of compact continuum structures in Arp 220 still remains open. Although a starburst, as exemplified by the existence of radio supernovae, can explain Arp 220s bolometric luminosity (Smith et al. 1998), the hard X-Ray emission spectrum and spatial distribution show that they are unlikely to be its main power source and other alternatives are proposed, for example several Ultra-Luminous X-Ray sources (ULX) or one (or several) low-mass AGN (Clements et al. 2002). The very high velocity gradient found in the southwestern maser (Figure 7b) marks it as a possible candidate to host a ULX or a low mass ($\sim 1.7 \times 10^7 M_\odot$) AGN. The sites of the radio supernovae are of very small extent and show very faint maser emission, so it is not feasible to study velocity gradients in these regions. Long time monitoring and analysis of their light curves is needed for their properties to be revealed in detail.

REFERENCES

Baan W. A., 1985, Nature, 315, 26
Baan W. A., Haschick A. D., 1984, ApJ, 279, 541B
Baan W. A., Haschick A. D., 1995, ApJ, 454, 745B
Baan W. A., Wood P. A. D., Haschick A, D., 1982, ApJ, 260, L49
Barnes J. E., 2002, MNRAS, 333, 481B
Bressan A., Silva L., Granato G. L., 2002. A&A, 392, 377B
Carilli C. L., Taylor G. B., 2000, ApJ, 532L, 95C
Carilli C. L., Wrobel J. M., Ulvestad J. S., 1998, AJ, 115, 928C
Clements D. L., MacDowell J. C., Shaked S., Baker A. C., Borne K., Collina L., Lamb S., Mundell S., 2002, ApJ, 581, 974C
Darling, J., Giovanelli,R. 2002, AJ, 124, 100
Diamond P. J., Norris R. P., Baan W. A., Booth R. S., 1989, ApJ, 340L, 49D
Eckart A., Downes D., 2001, ApJ, 551, 730E
Iwasawa K., Matt G., Guainazzi M., Fabian A. C., 2001, MNRAS, 326, 894I
Lonsdale Colin J., Diamond P. J., Smith H. E., Lonsdale Carol J., 1998, ApJ, 493L, 13L
Lonsdale Colin J., Diamond P. J., Smith H. E., Lonsdale Carol J., 2001, IAU Symp. 206
Momjian E., Romney J. D., Carilli, C. L., Troland T. H., Taylor G. B., 2003 in preparation
Mundell C. G., Ferruit P., Pedlar A., 2001, ApJ, 560, 168M
Norris R. P., 1988, MNRAS, 230, 345N
Philström Y. M., Conway J. E., Booth R. S., Diamond P. J., Polatidis A. G., 2001, A&A, 377, 413P
Sakamoto K., Scoville N, Z., Yun M. S., Crosas M., Genzel R., Tacconi L. J., 1999, ApJ, 514, 68S
Sanders D. B., Mirabel I. F., 1996, ARA&A, 34, 749S
Scoville N. Z., Yun M. S., Bryant P. M., 1997, ApJ, 484, 702S
Scoville N. Z. et al., 1998, ApJ, 492L, 107S
Shioya Y., Trentham N., Tanigushi Y., 2001, ApJ, 548L, 29S
Smith H. E., Lonsdale Carol J., Lonsdale Colin J., Diamond P. J., 1998, ApJ, 493L, 17S
Soifer B. T., Sanders D. B., Madore B. F., Neugebauer G., Danielson G. E., Elias J. H., Lonsdale Carol J., Rice W. L., 1987, ApJ, 320, 238S
Taylor G. B., Silver C. S., Ulvestad J. S., Carilli C. L., 1999, ApJ, 519, 185
Ulvestad J. S., Wrobel J. M., Roy A. L., Wilson A. S., Falcke, H., Kirchbaum T. P., 1999, ApJ, 517L, 81U
Xia X. Y., Xue S. J., Mao S., Boller Th., Deng Z. G., Wu H, 2002, ApJ, 564, 196X
Yates J. A., Richards A. M. S., Wright M. M., Collett J. L., Gray M. D., Field D., Cohen R. J., 2000, MNRAS, 317, 28Y

ACKNOWLEDGMENTS

MERLIN is a national facility operated by the University of Manchester at Jodrell Bank Observatory on behalf of PPARC.

E. Rovilos would like to thank the Greek State Scholarships Foundation, without its financial support this work would not have been possible. We thank Al Stirling and Rob Beswick for useful discussions.